POLITECNICO
MILANO 1863

SCUOLA DI INGEGNERIA INDUSTRIALE
E DELL'INFORMAZIONE

Executive Summary of the Thesis

Admissible Region Approach to Correlate Measurements Tracks to Satellite Fragmentation Events

Laurea Magistrale in Space Engineering - Ingegneria Spaziale

Author: Alessandro Mignocchi

Advisor: Prof. Marco Felice Montaruli

Co-advisor: Prof. Pierluigi Di Lizia

Academic year: 2022-2023

1. Introduction

Recent years have seen a fast increase in space traffic: the growing in-orbit population of satellites has led to an impressive increasing threat of potential collisions. Breakup events are not so uncommon: they include explosions, crashes, or anomalous events resulting in fragmentation, and they represent the dominant source of objects in the Near-Earth environment [1].
In this context, it is extremely important to detect new fragmentation or assign newfound fragments to the corresponding parent, to mitigate the collision risk and increase the safety of newly designed space missions [2]. However, algorithms implemented for these operations struggle when the observations of fragments are insufficient to determine their orbit accurately.
The present thesis illustrates two newly developed algorithms, the Topocentric Intersection Theory Analysis (TITA) and the Orbital Parameters Intersection Analysis (OPIA), dedicated to the correlation of fragments observations to breakup events. Their innovative aspect lies in the use of the admissible region tool, which allows to carry out this operation without requiring any result of Initial Orbit Determination (IOD) of the fragment.

2. Admissible Region

In this section, a review of the admissible region tool is offered.
This concept was introduced to handle too-short arcs where classical methods for IOD failed, gathering all the information available to extract the maximum potential from ground-based observations [3]. In particular, the focus of this work is posed on the optical case, as the implemented algorithms employ optical measurements. However, this does not exclude possible future developments in the radar case [4].

2.1. Observations and attributable

Considering a topocentric spherical system centered in the ground-based optical observer, it is possible to define $(\rho, \alpha, \delta) \in \mathbb{R}^+ \times [0, 2\pi) \times (-\pi/2, \pi/2)$ as the topocentric spherical coordinates of an Earth satellite, where the angular coordinates (α, δ) can be expressed with respect to an arbitrarily topocentric reference system. Here, α represents the right ascension and δ the declination, defined with respect to the J2000 reference, centered in the observer. The value of the range is indicated with ρ, expressing the linear distance between the observer and the orbiting satellite.

When an optical survey is carried out, it is common to retrieve an angular track, which consists of a batch of angular observations. This information is usually preliminary processed through a procedure called track compression, in-depth illustrated in Sec. 2.2.
In this way, it is possible to define the *optical attributable* vector as in Eq. 1:

$$\mathcal{A}_{opt} = (\alpha, \delta, \dot{\alpha}, \dot{\delta}) \in [0, 2\pi) \times (-\pi/2, \pi/2) \times \mathbb{R}^2 \tag{1}$$

This vector is precisely the set of coordinates that can be measured from the observer's frame on the Earth's surface, provided with the inertial angular location of the observatory to define the ground station position and velocity at the time of measurements.
$\mathcal{A}_{opt}$ is essentially a 4-dimensional vector in the measurements space. However, computing a complete orbit requires six parameters, and information on two additional quantities is needed: range ρ and range-rate $\dot{\rho}$.

2.2. Observations compression

To define the angular rates and complete the optical attributable $\mathcal{A}_{opt}$, optical tracks need to be processed. This strategy is known as track compression, which is a basic pre-processing technique that consists in transforming a set of observations collected by a sensor (i.e., track) into a single one, at the middle epoch of the observation [5, 6]. The benefits of this process are three:

1. Mitigation of measurements noise effect.
2. Reduction of the number of measurements.
3. Estimation of measurement rates ($\dot{\alpha}$ and $\dot{\delta}$).

This compression can be achieved by a least-squares low degree fit of the observation track, while the rate of change of a measurement is obtained by deriving the regression polynomial.
In this work, the angular information is extracted from a Tracking Data Message (TDM), and regression polynomials are generated up to the tenth order, to avoid badly conditioned behavior. Then, the most suitable polynomial is found through a test on the R-squared (R^2) value. The R^2 variant implemented is the one illustrated in Eq. 2, where y_i represents the n observation measures, while f_i is the i-th polynomial evaluation at the same epoch.
Finally, the polynomial characterized by the minimum R^2 value is evaluated at the middle epoch of observation to save the single angular value from the track, while the angular rate is obtained from the first-order derivative evaluated at the same time.

$$\bar{y} = \frac{1}{n}\sum_i y_i \longrightarrow R^2 = 1 - \frac{\sum_i (y_i - f_i)^2}{\sum_i (y_i - \bar{y})^2} \tag{2}$$

A practical example is illustrated in Fig. 1, where the observation compression is performed on an optical track recorded by a ground station.

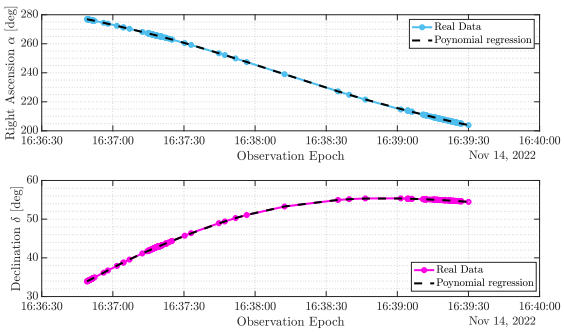

Figure 1: Optical observation tracks and regression polynomials.

2.3. Admissible region

The admissible region concept is a mathematical formulation describing a two-dimensional surface in the measurements space, such that the possible constraints on the orbital parameters of the observed object are satisfied. Imposing these conditions, the admissible region represents the locus of points of meaningful values in the measurements space.
The admissible region tool is founded on the knowledge of the attributable, derived from the compression of an optical track. The surface extends into the measurements space where the values have not been fixed by the corresponding attributable, i.e. in the $(\rho, \dot{\rho})$-plane for the optical case.
Given the optical attributable $\mathcal{A}_{opt}$, the idea is to derive physical constraints on quantities dependent on the range and range rate. Starting from the specific geocentric energy in Eq. 3, it is possible to impose the main orbital requirements listed below, introduced by Farnocchia et al. in [7].

$$\mathcal{E}(\rho, \dot{\rho}) = \frac{1}{2}\,||\dot{\mathbf{r}}(\rho, \dot{\rho})||^2 - \frac{\mu}{||\mathbf{r}(\rho)||} \tag{3}$$

- Specific energy: $\mathcal{C}_1 = \{(\rho, \dot{\rho}) : \mathcal{E} \leq 0\}$.
- Range: $\mathcal{C}_2 = \{(\rho, \dot{\rho}) : \rho_{min} \leq \rho \leq \rho_{max}\}$.
- Semi-major axis: $\mathcal{C}_3 = \{(\rho, \dot{\rho}) : a \leq a_{max}\}$.
- Eccentricity: $\mathcal{C}_4 = \{(\rho, \dot{\rho}) : e \leq e_{max}\}$.

The final admissible region is then defined as a subset of the $(\rho, \dot{\rho})$-plane by the condition:

$$\mathcal{C} = \bigcap_{i=1}^{4} \mathcal{C}_i \tag{4}$$

An example of the optical admissible region is illustrated in Fig. 2, where the energy and semi-major axis constraints are represented, as well as the one on the maximum eccentricity and the minimum range.

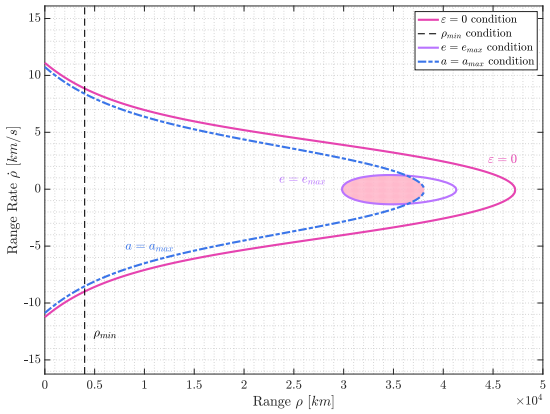

Figure 2: Optical admissible region, painted in *pink*.

Sampling this area with a finite number of points allows to obtain meaningful couples of $(\rho, \dot{\rho})$ with which completing the initial optical attributable in the 6-dimensional measurements space $[\alpha, \delta, \dot{\alpha}, \dot{\delta}, \rho, \dot{\rho}]$. After the conversion to the Cartesian space (possible only if the observer geocentric position $\mathbf{q}$ is available), a set of admissible Cartesian states $\mathbf{x}_i$ are obtained, starting from a single observation and without carrying out any Orbit Determination (OD) process.

3. Method

This section outlines the core methodologies employed in the development and implementation of two algorithms, tailored to correlate fragments optical tracks to their respective fragmentation events.

3.1. TITA analysis

The TITA linkage methodology was proposed by Maruskin et al. [8] as a future development of their work in the track-to-track correlation problem, and is here adapted to the track-to-fragmentation case.

Let's consider the breakup of a space object orbiting around the Earth, whose blast-point state $\mathbf{x}^{blast}$ and epoch t_{blast} have already been characterized. Some hours later, at t_{obs}, one object is detected by an optical ground station, recording a TDM. The final objective is to assess whether the object is correlated to the detected fragmentation event.

The optical attributable of the observed object $\mathcal{A}_{opt}^{obs}$ is extracted from the TDM, and the corresponding admissible region is found and sampled at t_{obs}. Provided the observer geocentric position $\mathbf{q}^{obs}$ and velocity $\dot{\mathbf{q}}^{obs}$, the admissible attributable found are converted from measurements to Cartesian space, generating multiple Virtual Debris (VDs), and then propagated backward in time to t_{blast}.

To characterize the measurements space at t_{blast}, a virtual ground station is projected on the Earth's surface from the real position of the fragmentation $\mathbf{p}^{blast}$, to simulate a near-Zenith observation of the event. In particular, the latitude ϕ and longitude λ of the fragmentation projection are modified adding one degree to avoid an observation completely at the Zenith, and the geographical coordinates of the station are found as:

$$\begin{aligned} \phi_{station} &= \phi_{frag} + 1\,\text{deg} \\ \lambda_{station} &= \lambda_{frag} + 1\,\text{deg} \end{aligned} \tag{5}$$

Here the filtering phase begins, which consists in a reachability analysis that correlates the observed object only if, at t_{blast}, any VD approaches the fragmentation position both in the Cartesian and measurements space. Note that the compatibility conditions regard only position-dependent quantities, since parent object and fragments had different velocities at t_{blast}. The filter is divided into three consecutive pruning steps, where one VD can have access to subsequent levels only if satisfies the previous conditions:

1. **Cartesian step**: the Cartesian distance between the positions of VDs and parent object is evaluated at t_{blast} and, if above a certain threshold, the samples are filtered out:

$$||\mathbf{p}^{blast} - \mathbf{p}_i^{blast}|| \frac{1}{R_E} \leq \varepsilon_{cart} \tag{6}$$

2. **Measurements step**: surviving samples are converted again measurements space and enter in a triple-level waterfall structure, in which three pruning conditions are placed in series:
   - Condition on the right ascension α: $|\alpha - \alpha_i| \leq \varepsilon_\alpha$
   - Condition on the declination δ: $|\delta - \delta_i| \leq \varepsilon_\delta$
   - Condition on the range ρ: $|\rho - \rho_i| \dfrac{1}{R_E} \leq \varepsilon_\rho$
3. Δv **step**: the velocity compatibility between VDs passing the filter and the parent object at the fragmentation epoch is checked. The norm of the difference between the Cartesian velocities is computed and, once again, compared to a maximum value of Δv that can occur in a fragmentation event:

$$\Delta v = ||\mathbf{v}^{blast} - \mathbf{v}_i^{blast}|| \leq \Delta v_{max} \quad (7)$$

If this last test is also positive for at least one of the propagated VDs, the observed object is considered *correlated* to the fragmentation event. If at the end of the filtering phase no VD remains, the object is considered *uncorrelated*.

3.2. OPIA analysis

OPIA is the second algorithm developed for the correlation of observations to a fragmentation event, exploiting a more statistical-focused approach than TITA. The algorithm preserves the key features of the admissible region tool, handling too-short arcs without OD results, but the analysis is performed in the orbital elements space, with particular focus on the inclination i and on the right ascension of the ascending node RAAN.
These parameters describing the orbital plane exhibit very slow variations due to orbital perturbations, connected to the J_2 nodal regression for the RAAN and to the third body perturbation for the inclination, and even during a fragmentation event many fragments preserve inclination and RAAN similar to those of the parent object.
Similar to TITA (Sec. 3.1), the starting point of OPIA algorithm is represented by the known fragmentation event $\{\mathbf{x}^{blast}, t_{blast}\}$ and the TDM recorded by an optical ground station at t_{obs}. Once again, the optical attributable is extracted from the TDM and the related admissible region is characterized and sampled at t_{obs}.
Samples are then converted to the Cartesian space and propagated up to t_{blast}. This last step can be skipped to obtain an algorithm free from the propagation process, taking advantage of the low sensitivity of inclination and RAAN to orbital perturbations to develop the same analysis described below at t_{obs}.
From the propagated admissible states $\mathbf{x}_i^{blast}$ it is possible to compute the Keplerian parameters of VDs at t_{blast}, whose distribution can be characterized on the (i, Ω)-plane. The shape of the distribution is described through the Gaussian (or normal) assumption, so that the sample mean $\boldsymbol{\mu}_{\mathrm{VD}}$ and covariance $\boldsymbol{\Gamma}_{\mathrm{VD}}$ can be computed.
Focusing now on the parent object state $\mathbf{x}^{blast}$ at the fragmentation epoch t_{blast}, it is possible to apply the NASA Standard Breakup Model [9] to find the synthetic distribution of simulated fragments after the event. In this way, Virtual Fragments (VFs) states $\mathbf{x}_k^{blast}$ are retrieved and converted into the Keplerian space, obtaining the VFs inclinations and RAAN on the (i, Ω)-plane. Also in this case, the distribution is described as Gaussian and the sample mean $\boldsymbol{\mu}_{\mathrm{VF}}$ and covariance $\boldsymbol{\Gamma}_{\mathrm{VF}}$ are computed.
The correlating phase consists in evaluating the statistical distance between the two distributions found at the previous points. This is done employing the Mahalanobis distance metric, and the main steps are:

- Computation of the squared Mahalanobis distance D^2 between the distributions:

$$D^2(\boldsymbol{\mu}_{\mathrm{VD}}, \boldsymbol{\mu}_{\mathrm{VF}}) = (\boldsymbol{\mu}_{\mathrm{VD}} - \boldsymbol{\mu}_{\mathrm{VF}})^T (\boldsymbol{\Gamma}_{\mathrm{VD}} + \boldsymbol{\Gamma}_{\mathrm{VF}})^{-1} (\boldsymbol{\mu}_{\mathrm{VD}} - \boldsymbol{\mu}_{\mathrm{VF}}) \quad (8)$$

- Characterization of the χ^2 critical value for the interval of confidence set (99.8%), through the MATLAB ® function `chi2inv`.
- Finally, finding the correlation index R (or coefficient) as $R = \left| \dfrac{D^2}{\chi^2} \right|$.

Eventually, if the computed correlation index R is below a certain threshold $R_{max} = 1$ the object is *correlated* to the fragmentation event, otherwise the object is considered *uncorrelated*. An example of a positive correlation is depicted in Fig. 3.
As introduced previously, the algorithm works in the same way even if VDs propagation is avoided

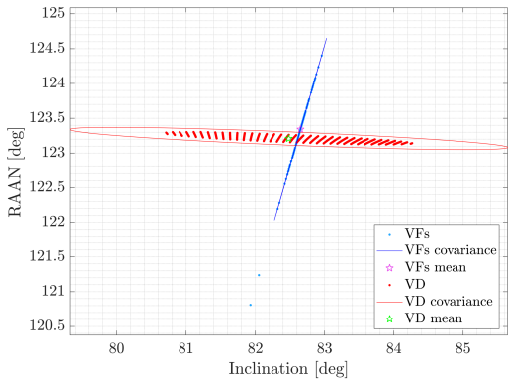

Figure 3: Means and covariances on (i, Ω)-plane of the virtual debris and virtual fragments distributions found at t_{blast}.

and $\boldsymbol{\mu}_{\text{VD}}$ and $\boldsymbol{\Gamma}_{\text{VD}}$ are found at t_{obs}, as the variations in inclination and RAAN are negligible in the time horizon considered in this analysis. For this reason, it is possible to focus on these quantities without performing propagation, i.e. comparing the parent and the fragment inclination and RAAN even if characterized at different times.
An important implication of the comment above is that it is possible to apply the NASA Standard Breakup Model starting from the last parent ephemeris $\{\mathbf{x}^{eph}, t_{eph}\}$, that is without performing any propagation of the parent object to the fragmentation epoch. As consequence, it is possible to perform the implemented analysis even if the fragmentation event is not characterized. Due to the low sensitivity of these orbital parameters, the VFs distribution in the (i, Ω)-plane can be considered accurate enough even if not performed at t_{blast}.
This allows to link the fragment and the parent before the characterization of the event itself, improving and speeding up the cloud monitoring process.

4. Simulations and Results

Here, the objective is to evaluate the effectiveness and accuracy of the algorithms developed through numerical simulations implemented in the MATLAB ® environment. It is illustrated how testing data sets are generated, as well as the basic performance of the codes and a final sensitivity analysis.

4.1. Data set generation

To test the performance and the accuracy of the implemented procedures, a fragmentation event needs to be simulated, to provide virtual observations of correlated fragments. This is done employing the NASA Standard Breakup Model, which allows to retrieve a representative set of fragments just after the event, available for the propagation and observation simulation.
It is worth to point out that also space objects not related to the event need to be generated to test the ability of the algorithm in avoiding wrong associations and, for this purpose, the Space-Track site is exploited to obtain TLEs of generic satellites, represented in Fig. 4 for the GEO scenario. By this way, a space object catalogue is defined, including both simulated fragments and satellites not related to the breakup. The numerical simulation processes this catalogue to investigate for possible correlations to an alerted fragmentation event.
The performance analysis is conducted both with LEO and GEO scenarios, to verify the sensitivity of the algorithms to the orbital region. For this reason, two different data sets, represented in Tab. 1, are generated.

	Sim. Fragments	No fragments
LEO	237	2919
GEO	237	798

Table 1: Space objects catalogue considered in the analysis. It includes both simulated fragments and satellites not related to the breakup.

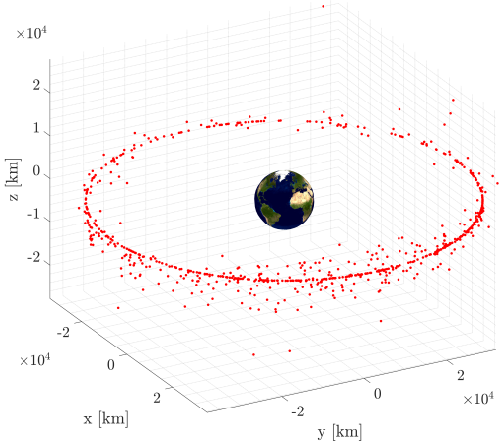

Figure 4: GEO satellites tracked on Space-Track, employed as no-related objects.

4.2. Nominal performance

Starting from TITA, the performance of the algorithm is represented by the percentage of fragments correctly correlated, that are classified as true positives, as well as the percentage of no-related catalogued objects excluded, classified as true negatives.
Note that the values of the filtering thresholds are set through an initial tuning phase, performed for the main orbital regions under analysis (LEO and GEO), and resulting in the values shown in Tab. 2.

	LEO	GEO
ε_{cart} on position	191 km	637 km
ε_{α} on right ascension	8.31 deg	0.43 deg
ε_{δ} on declination	8.31 deg	0.0115 deg
ε_{ρ} on range	159 km	191 km
Δv_{max} on velocity	500 m/s	500 m/s

Table 2: TITA filtering thresholds derived from the tuning process in LEO and GEO.

TITA outcomes are illustrated in Tab. 3.

	LEO	GEO
True positives	89.03%	89.87%
False negatives	10.97%	10.13%
True negatives	100.00%	96.21%
False positives	0.00%	3.79%

Table 3: TITA nominal correlation performance.

The results in LEO and GEO are similar, demonstrating association ability and excellent performance in excluding the correlation of objects not related to the event. However, it is easier to investigate the nature of false positives in GEO. TITA performance is closely related to the geometric proximity of the propagated samples with the parent object at t_{blast}. As depicted in Fig. 4, GEO satellites are characterized by very similar orbital planes and, for this reason, it is more likely that the propagation of no-related objects ends up in the fragmentation zone. Furthermore, the relationship between wrongly excluded fragments and a high Δv magnitude is clearer in GEO rather than in LEO.

In conclusion, the performance of TITA is more predictable and clear in GEO than in LEO.
For a fair comparison, OPIA is also tested in both LEO and GEO on the same fragmentation scenarios on which TITA is tested, and the results are presented in Tab. 4. The outcomes presented do not include the propagation step since this reduces the computational cost without causing a degradation in accuracy.

	LEO	GEO
True positives	99.16%	99.58%
False negatives	0.84%	0.42%
True negatives	100.00%	42.35%
False positives	0.00%	57.65%

Table 4: OPIA nominal correlation performance.

OPIA shows unparalleled accuracy and effectiveness in correlating objects in the LEO environment, where the main source of false negatives is a large component of Δv, appreciable from the degradation of the correlation index as a function of the velocity change magnitude in Fig. 5.

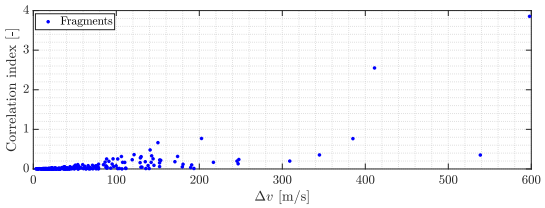

Figure 5: Correlation index distribution as a function of the velocity change between real fragments and parent object in LEO.

In LEO, it is also interesting to observe the distribution of the correlation coefficients with respect to the RAAN of the correlated fragments in Fig. 6, reproducing the quadratic behavior imposed by the χ^2-test and expressed in Eq. 8. Fragments with inclination and RAAN closer to the parent ones present a smaller correlation index, favoring the association process.
However, an increase of false positives can be noticed in GEO. This is mainly due to the orbital similarity of objects in the GEO region, where the satellites share similar inclination and RAAN. This makes OPIA algorithm prone to

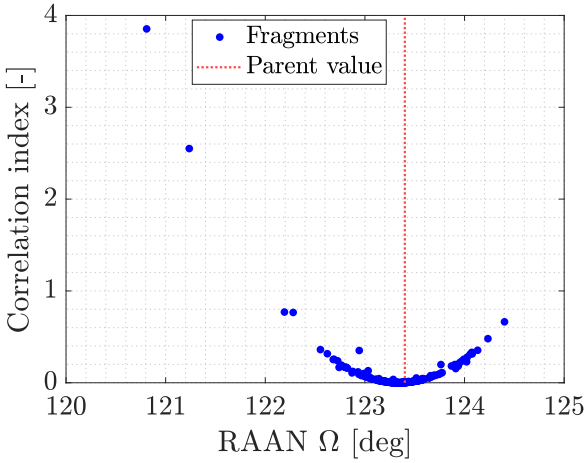

Figure 6: Correlation index distribution as a function of the real fragments RAAN in LEO.

false associations.
Results demonstrate that TITA can operate in both LEO and GEO, offering satisfactory accuracy, even if not excellent. OPIA provides unparalleled precision and efficiency in LEO, while in GEO it is prone to false association of no-related objects to the event. For this reason, the two algorithms presented reveal to be complementary rather than competitive, and their joint use can accurately cover both LEO and GEO regions.

4.3. Sensitivty analysis

The tests presented herein are designed to emulate the real-world challenges that these algorithms may encounter, and to highlight which of the following elements negatively affect their results:

- **Measurements noise**: noises on optical measurements can introduce a modeling fallacy in the optical admissible region.
- **Error on parent position**: a wrong evaluation of the parent position at the fragmentation epoch can represent an additional source of mismatching between observed fragments and the parent object.
- **Error on fragmentation epoch**: an error on the time of fragmentation can negatively affect the correlation process, especially for algorithms that perform propagation from or to that date.
- **Number of points in the sampling grid**: the smaller the number of samples used, the shorter the computational time is, but also the less accurate the admissible region representation is.
- **Orbital perturbations**: a non-Keplerian propagation introduces short and long terms effects on objects orbital parameters.

Given the results obtained in the previous section, this analysis is only performed in LEO for OPIA and in GEO for TITA, i.e. where they respectively demonstrate a promising performance. This is also done to avoid analyzing the robustness of the code where it is not performing.
Table 5 offers a summary of the overall performance of the codes under the influence of perturbations.

Robustness to	OPIA	TITA
Measurements noise	✓	✓
Error on parent position	✓	✓
Error on frag. epoch	✓	×
Number of sampling points	✓	×
Orbital perturbations	✓	✓

Table 5: Summary comparison of OPIA (LEO) and TITA (GEO) robustness.

On the one hand, OPIA results robust to all the sensitivity analysis conducted, thus confirming its performance in LEO region. It is worth to remark that orbital perturbations do not affect the method, as the method does not need any propagation. On the other hand, TITA can handle measurements noise, errors on the parent position, and orbital perturbations, but it is sensitive to errors on the fragmentation epoch and to the number of points of the sampling grid, and this is reasonable, since the method is based on the propagation up to the fragmentation epoch and on the number of samples surviving at the end of the filtering phases.

5. Conclusions

After an in-orbit breakup, uncorrelated tracks acquired by on-ground means shall be processed to verify their association to the event. To this end, two approaches were developed, resulting in two algorithms that together ensure satisfactory performance both in LEO and GEO. TITA and OPIA base their track-to-fragmentation process on the admissible region formulation, which allows to handle very short observational arcs, even where the classical method for IOD

fail. The most innovative aspect lies precisely in the association process, which can be verified without having to determine the orbit of the fragment.
On the one hand, OPIA exploits the similarity of inclination and RAAN of the admissible region samples and guarantees excellent accuracy in LEO, but presents deteriorated performance in GEO, as the similarity between the above-mentioned orbital parameters in the objects catalogue lead to many false associations. Furthermore, it features robustness in off-nominal situation, and does not require orbital propagation, allowing for faster computation.
On the other hand, TITA is based on the geometrical proximity between the fragment samples and the parent object both in the Cartesian and measurements spaces, offering a good, but not optimal, performance in LEO and GEO. In particular, in LEO region it is less performing than OPIA. On the contrary, TITA is more performing in GEO, and, for this reason, it is considered as a complementary algorithm to OPIA.

Future development paths may focus on analyzing the OPIA performance into the GEO region, investigating the possibility to exploit a convenient orbital state representation, such as that of Delaunay [8].
Furthermore, the operations of TITA and OPIA can be extended to the radar case, adapting the procedures to the radar admissible region characteristics.
However, the potential of these algorithms could lead to developments far beyond the simple fragment-event association: with a time-variant analysis, it would be interesting to investigate if these tools can prove to be a basis for algorithms dedicated to the characterization of fragmentation events, starting from a single fragment observation and without IOD results.

References

[1] A. Muciaccia, L. Facchini, M.F. Montaruli, and G. Purpura et al. Observation and analysis of Cosmos 1408 fragmentation. *73rd International Astronautical Congress (IAC)*, 2022.

[2] M. Romano, A. Muciaccia, M. Trisolini, P. Di Lizia, C. Colombo, A. Di Cecco, and L. Salotti. Puzzle software for the characterization of in-orbit fragmentations. *8th European Conference on Space Debris*, 2021.

[3] A. Milani, G.F. Gronchi, M. Dè Michieli, and Z. Knezevic. Orbit determination with very short arcs: I admissible regions. *Celestial Mechanics and Dynamical Astronomy*, 90:59–87, 2004.

[4] M.F. Montaruli, L. Facchini, P. Di Lizia, M. Massari, G. Pupillo, G. Bianchi, and G. Naldi. Adaptive track estimation on a radar array system for space surveillance. *Acta Astronautica*, 198:111–123, 2022. doi:10.1016/j.actaastro.2022.05.051.

[5] A. Pastor, M. Sanjurjo-Rivo, and D. Escobar. Track-to-track association methodology for operational surveillance scenarios with radar observations. *Celestial Mechanics and Dynamical Astronomy*, 2022. doi:10.1007/s12567-022-00441-4.

[6] L. Pirovano, D.A. Santeramo, R. Armellin, P. Di Lizia, and A. Wittig. Probabilistic data association: the orbit set. *Advanced Maui Optical and Space Surveillance Technologies Conference (AMOS)*, 132, 2020. doi:10.1007/s10569-020-9951-z.

[7] D. Farnocchia, G. Tommei, A. Milani, and A. Rossi. Innovative methods of correlation and orbit determination for space debris. *Celestial Mechanics and Dynamical Astronomy*, 107, 2010. doi:10.1007/s10569-010-9274-6.

[8] J.M. Maruskin, D.J. Scheeres, and K.T. Alfriend. Correlation of optical observations of objects in earth orbit. *Journal of Guidance, Control, and Dynamics*, 2009. doi:10.2514/1.36398.

[9] N.L. Johnson, P.H. Krisko, J.C. Liou, and P.D. Anz-Meador. NASA's new breakup model of evolve 4.0. *Advances in Space Research*, 28:1377–1384, 2001.